symmetry

MDPI

Article

New Tribological Aspects in the Micro-Areas of the Symmetric Rolling-Sliding Contact

Antoni John [1], Henryk Bakowski [2], Ioan Száva [3] and Sorin Vlase [3,4,*]

[1] Department of Computational Mechanics and Engineering, Faculty of Mechanical Engineering, Silesian University of Technology, Konarskiego 18A, Room 102, 44-100 Gliwice, Poland; antoni.john@polsl.pl
[2] Faculty of Transport, Silesian University of Technology, Krasińskiego 8, 40-019 Katowice, Poland; henryk.bakowski@polsl.pl
[3] Department of Mechanical Engineering, Transilvania University of Brasov, B-dul Eroilor, 29, 500036 Brasov, Romania; apukam27@gmail.com or eet@unitbv.ro
[4] Romanian Academy of Technical Sciences, B-dul Dacia 26, 030167 Bucharest, Romania
* Correspondence: svlase@unitbv.ro; Tel.: +40-722-643020

Abstract: The study of wear that occurs during operation in the wheel–rail assembly is a difficult process to analyze. The phenomena that accompany the wear process are extremely complex and involve many factors, which vary greatly over different periods of time and at different times of wheel–rail contact. Estimating the behavior of the system and its wear in operation is difficult to obtain. However, for common engineering applications, for which the determining factors, such as road profile, load, skid, speed and weather conditions, are known, useful results can be obtained by laboratory tests or by numerical simulation. The article aims to model the complex phenomena that take place in the rail wheel system, taking into account the impact that most essential operational factors have. For this, the Finite Element Method (FEM) is used, thus, trying to explain the wear mechanisms of the wheel–rail system. The obtained results are verified in the laboratory. The main observation in the paper refers to the fact that in the areas of maximum stress and deformation, cracks appear at the micro scale. FEM proved to be a method that can predict the appearance of these microcracks, the experimental results validating the numerical experiments. The research offers results that can prove to be of great importance in practice, for the analysis and improvement of railway safety.

Keywords: wear; microcontact rolling–sliding; FEM; tribological test; microtomography

check for updates

Citation: John, A.; Bakowski, H.; Száva, I.; Vlase, S. New Tribological Aspects in the Micro-Areas of the Symmetric Rolling-Sliding Contact. *Symmetry* **2022**, *14*, 1523. https://doi.org/10.3390/sym14081523

Academic Editor: Igor V. Andrianov

Received: 24 June 2022
Accepted: 21 July 2022
Published: 26 July 2022

1. Introduction

The system wheel–rail is a very complex system and the study of wear and the effect of different factors on this is a difficult process. Constant change and overlapping of various factors in a very short time represents reasons why the study of wear is hard to conduct [1,2]. However, thanks to the conducted simulation tests in the wheel–rail combination, it was possible to determine the wear mechanism depending on the limitations existing on the railroad track, e.g., load, slippage and speed, as well as atmospheric conditions, including the medium [3–8].

1.1. Influence of the Climate on Rolling–Sliding Contact

In the following, we try to offer a short synthesis on how climate particularities can influence the proposed phenomena, i.e., the rolling–sliding contact and, consequently, the wear magnitude.

Water presence in the wheel–rail contact is undoubtedly an important operating factor in the mechanism of wear. Thus, for the existence of water in the wheel–rail contact in Poland, according to the Central Statistical Office (GUS), from April to October, there are as many as 130 days of rainfall, i.e., the annual sum of rainfall is within the limits of

500–700 mm, which may be calculated as approximately 500–700 L per m^2. In most parts of Europe, the annual precipitation is 500–800 mm (500–800 L per m^2). In mountain areas, it is higher—usually 1000–2000 mm—also in the case of ranges and coasts particularly exposed to westerly winds from the ocean or seas 3000–4000 mm. About 500 mm and below falls on the south-eastern and eastern parts of the Balkan Peninsula, Apenian and Iberian Peninsula, the central and north-eastern parts of the Scandinavian Peninsula, in southern Ukraine and in the mountain-sheltered basins (in Old Castile even below 250 mm). In the European part of Russia, in the central belt, precipitation is mostly 400–600 mm and decreases toward the northeastern extremities to less than 300 mm, and in the Transcaspian Lowland, it falls even to 100–200 mm. In summer, in southern Europe, when it is overrun by tropical air masses, there is a dry season; precipitation occurs only in autumn and winter, and its maximum falls between September and December, only in northern Spain (in May). In the rest of Europe, precipitation is more evenly distributed over the year. In the west, cyclonic autumn–winter precipitation is more abundant, with the maximum between October and December. In Eastern Europe, Central Europe and the Scandinavian Peninsula, separated from the Atlantic by mountains, the summer convective precipitation is more effective. Their maximum falls in June (in the south of this part of Europe), in July (in the central belt) or in August (on the Scandinavian Peninsula) [9–12]. Attention should also be paid to the presence of water on the rolling surface of the railroad rails in the winter season, which is formed from standing snow. Thus, the influence of water has an important effect on the tribological behavior of the wheel–rail association, as it can penetrate into the resulting cracks and crevices in the surface layer of RCF (Figures 1 and 2) [13–19].

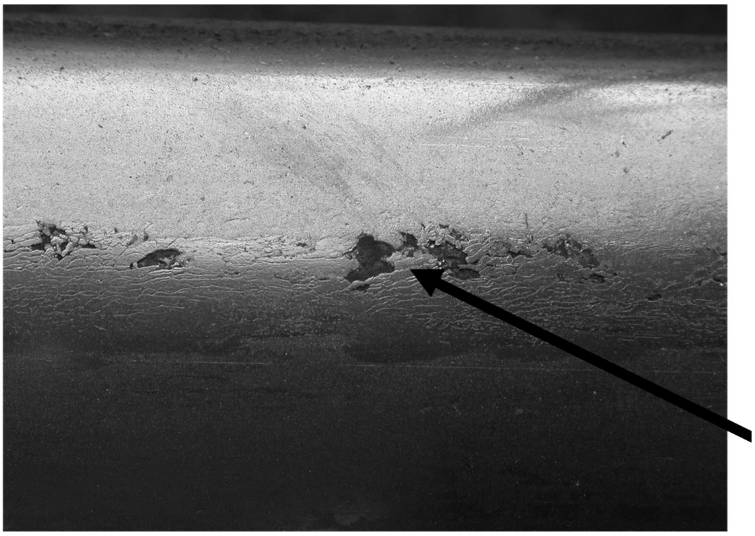

(**a**)

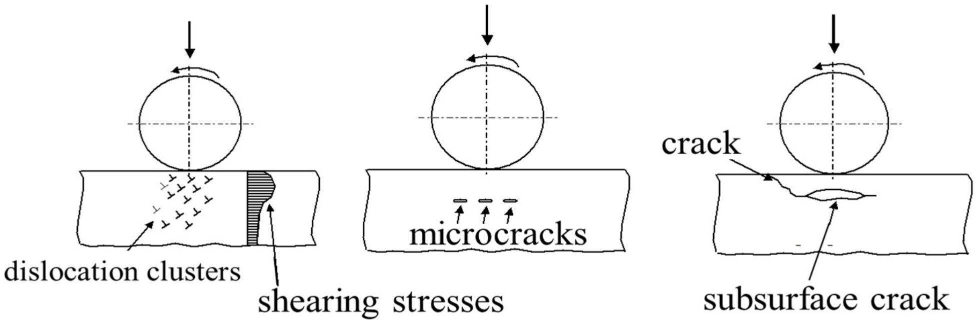

(**b**)

Figure 1. Delaminative nature of wear: (**a**) rolling surface of railroad rail, (**b**) wear model according to Suh's flake wear theory.

Figure 2. Delaminative nature of wear: wear of rails due to fluid closure in the gap.

Some data give us a picture of the level of precipitation in different parts of the world. In the USA, the level of precipitation is 767 mm (based on data collected by weather station provided by NOAA National Climatic Data Center). In Asia, precipitation is 2000 mm in the South, between 2000 and 3000 mm in the Southeast and between 7600 and 12,700 mm in the East (Britanica). In South America, the precipitation varies from 610 to 1420 mm per year and in Africa, less than 1000 mm per year (Britanica).

Of course, depending on the geographical area, connected with its local climate specific state, the magnitude of the water presence will be changed and, consequently, the wear process will be influenced. In the following, we will detail this very significant influence of the water's presence in the contact area on the wear magnitude, as well as on the lifetime diminishing.

1.2. Wear Presence Particular Influence on the Contact Area

To analyze the wear of the wheel–rail system, it is necessary to know what is the impact of the essential operational factors. Knowing these FEM factors becomes a very suitable method of analysis; within the FEM model, there is the possibility to introduce, as input data, the factors that influence the wear of the system. It is, thus, possible to obtain the stress field, which has a major influence on the wear phenomena. Thus, the areas where micro-cracks appear can be identified.

One of the many processes studied is the wear mechanism is the presence of a lubricating medium. For such a contact, apart from the effect of pitting and other types of wear, there is a phenomenon of fatigue crack propagation due to the spreading action of the fluid, which starts from the surface and leads inside to the material [20–27]. The cracking of the material inside the rail is due to stress propagation. This process is closely related to the so-called fluid confinement effect, whereby the fluid present in the crack is confined as it passes through the contact area. The fluid closure occurs as a result of the short-circuiting of the crack edges forced by the contact load when the walls inside the crack are bifurcated. It is assumed that at the moment of the crack edge closure (Figure 3), there is fluid between its bifurcated walls below the edge, which entered the crack interior from the external contact surface. When the crack is closed, there is a high fluid pressure inside the crack, which acts on the walls of the crack causing the crack to enlarge [28,29].

Water can penetrate through cracks and pores and, as a result, will increase the length of the subsurface fracture (Figures 4 and 5).

In Figures 3 and 4, we observed the cross-section perpendicular to the rail surface using intrusion material.

Rolling/sliding phenomena have long been studied due to the importance of the phenomenon in engineering applications. Numerous results have been published in older studies by various researchers [30–39].

The present study provides an explanation of the wear mechanism using FEM simulation tests.

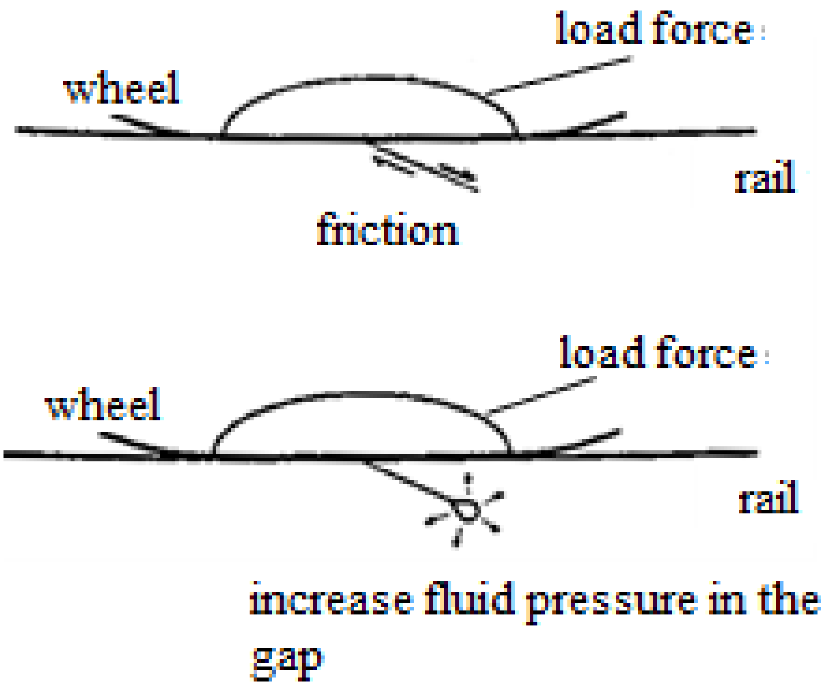

Figure 3. Schematic showing fluid confinement in a gap.

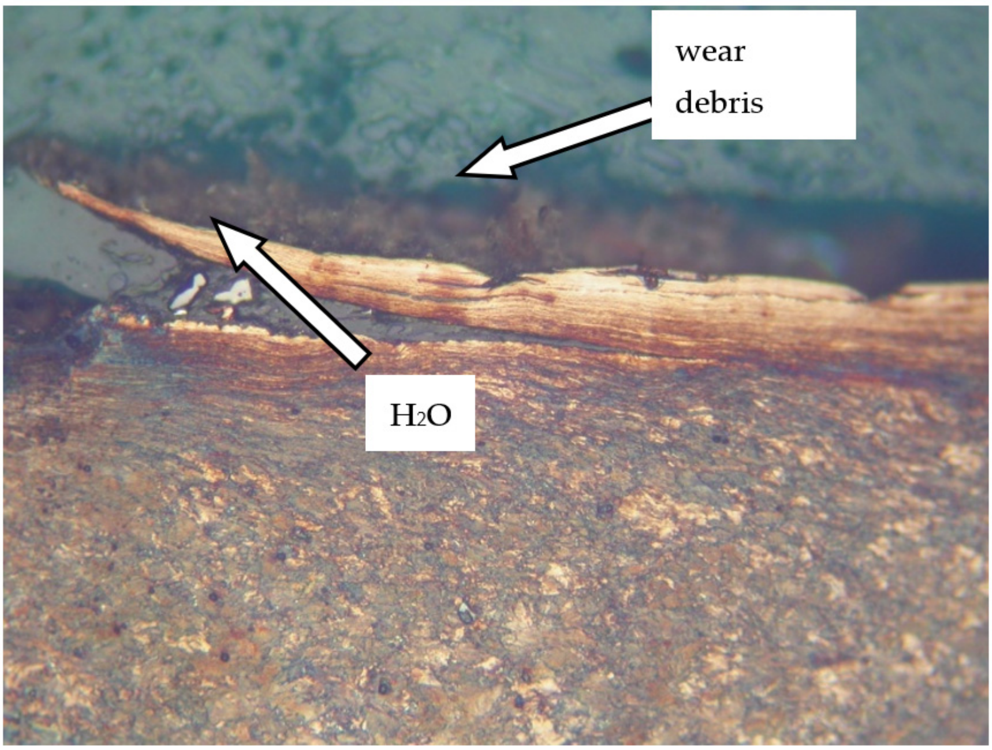

Figure 4. Detachable flaky wear debris into which a lubricating medium can penetrate in the gap.

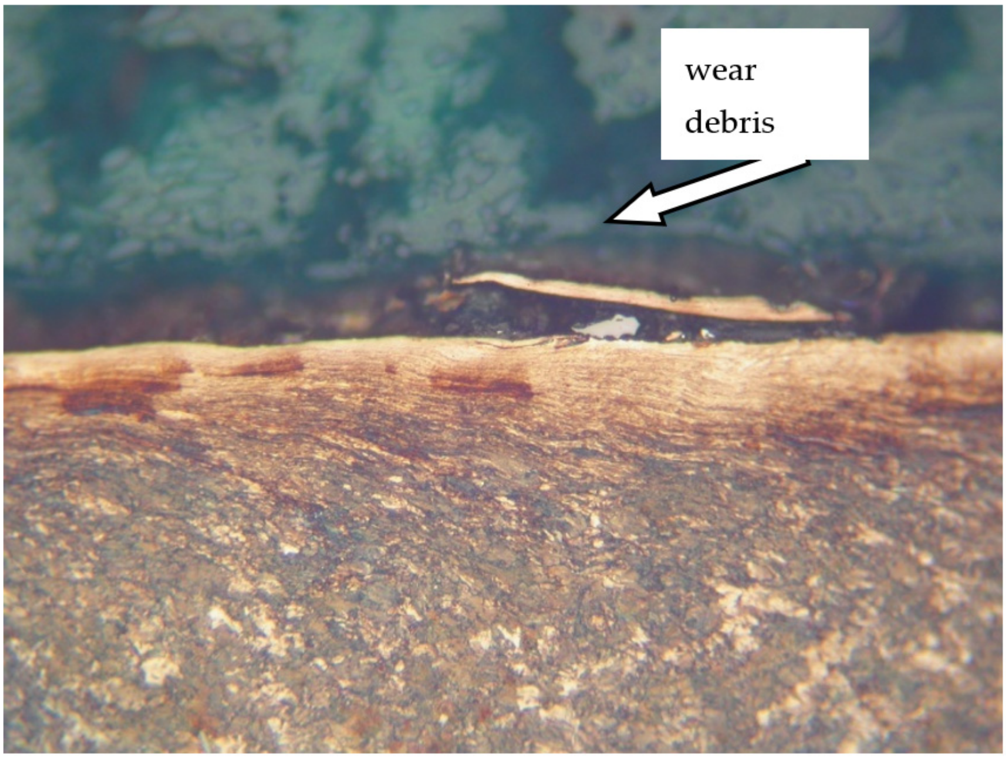

Figure 5. A detached piece of wear debris.

2. Materials and Methods

Numerical simulations using a computer microtomograph will allow locating the places most exposed to wear and damage depending on various operating conditions.

The wear phenomenon is a complex phenomenon; the wear residues have size and shape determined by the essential factors that intervene in the contact between the rail and the wheel. They may depend on the condition and properties of the surface layer of the materials in contact or the type of heat treatment of the material. For a pertinent analysis, all these factors and their role in the interaction that takes place must be considered [40–42].

One of the tasks undertaken in this paper is an attempt to explain the cause-and-effect relationship of operating parameters to the wear of the wheel/rail contact zone. To obtain a faithful reflection of the friction surface, the following procedure was used.

Data imported from a computer microtomograph (Figure 6) were processed using free software, FIJI. The images obtained under the microtomograph were saved in a lossless format (*.raw) in (*.stl) format. Using GMSH software, the geometric model allows you to generate a mesh and export to an MES solver (MSC.Marc). Figure 7 presents the stages of the procedure.

The subject of numerical simulations is analysis in the field of stresses in the contact zone for the real contact surface in the following sets of tests:

(a) Analysis of friction surface (deformable);
(b) Analysis of friction surface (deformable) and rigid ideal surface (rigid).

The analyzed model was a section of the friction surface with a width of 1.9 mm and a height not exceeding 16 μm. The tests were performed for 2D and 3D models. The MSC.Software/Marc system was used for numerical analysis. Non-linear calculations were performed. Rail material with the following material coefficients was assumed: Young's modulus E = 210,000 MPa and Poisson's ratio ν = 0.3 and a density ρ = 7900 kg/m^3. The detailed boundary conditions are illustrated in Figure 7. In the research, 453 (tri3) and 1942 (quad4) elements were used to build the model. In order to compare the obtained results, a model with a real contact surface was used (Figure 8).

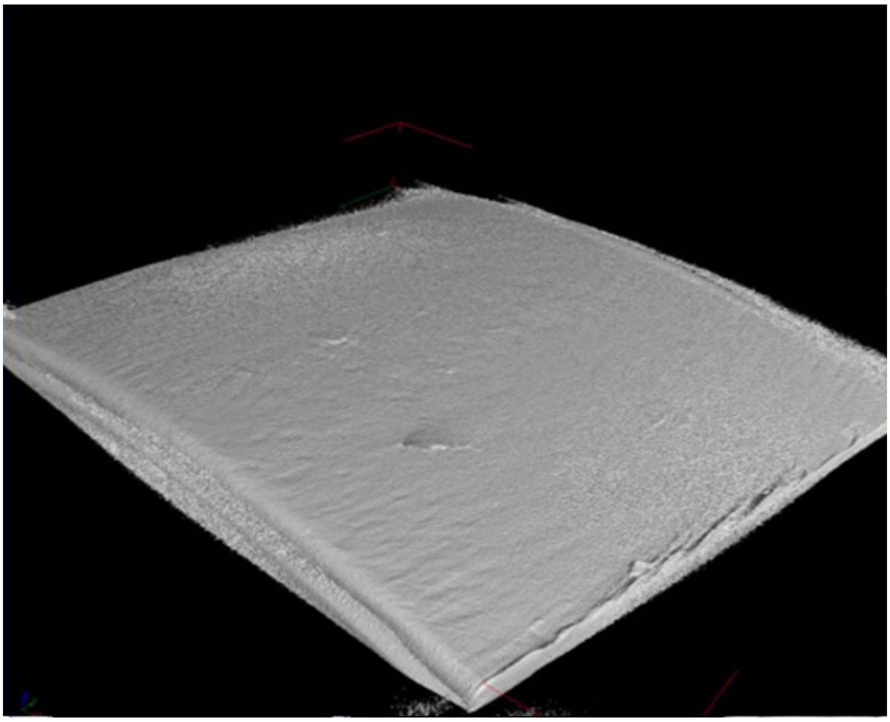

Figure 6. The real surface layer offered by Computed Tomography (Nanotom S).

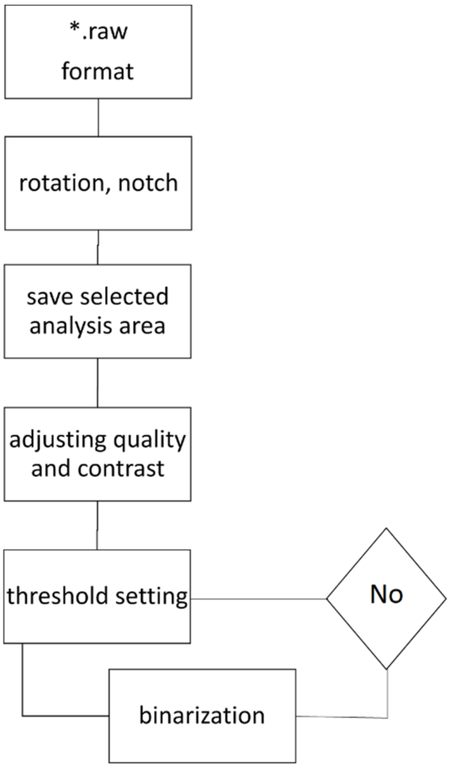

(**a**)

Figure 7. *Cont*.

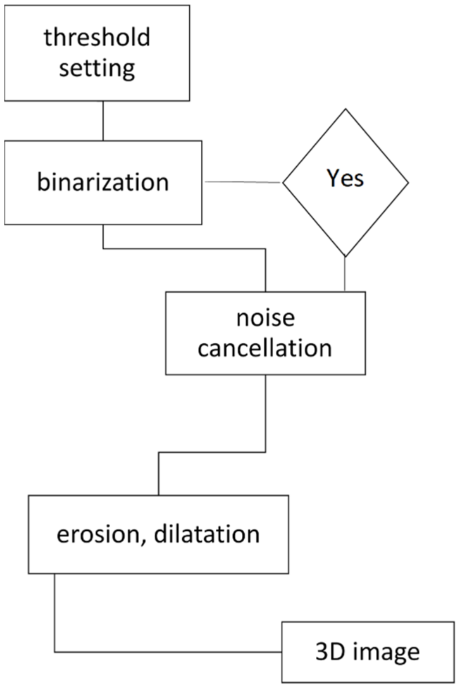

(**b**)

Figure 7. The stages of procedure: (**a**) beginning steps and (**b**) final steps.

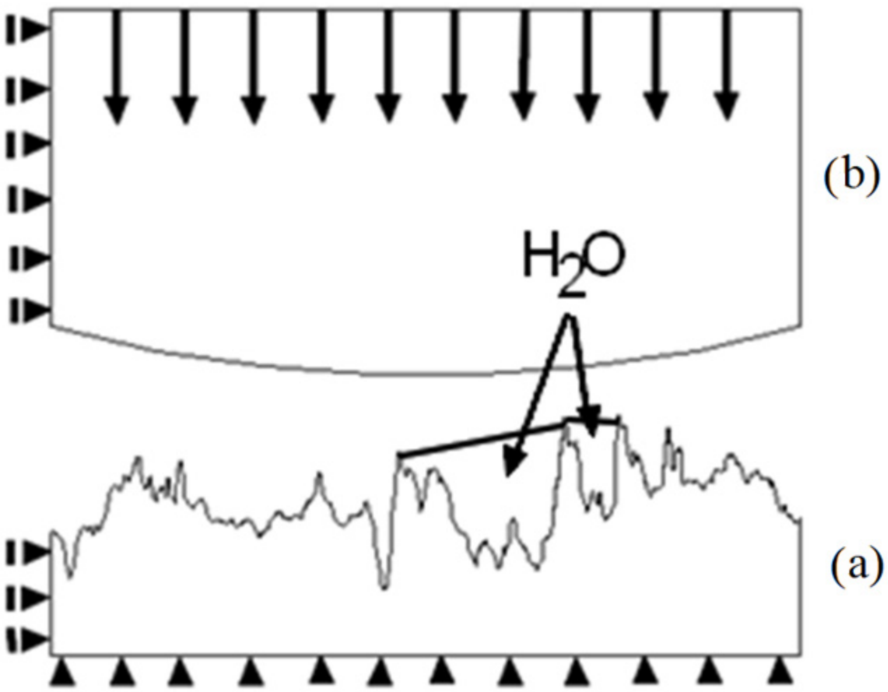

Figure 8. Boundary conditions: (**a**) real contact surface and (**b**) flat contact surface.

3. Results

From the experiments, we determined the contact area. As a result of the FEM analysis, the results of simulation tests are presented in Figure 9. Table 1 presents a summary of the obtained results.

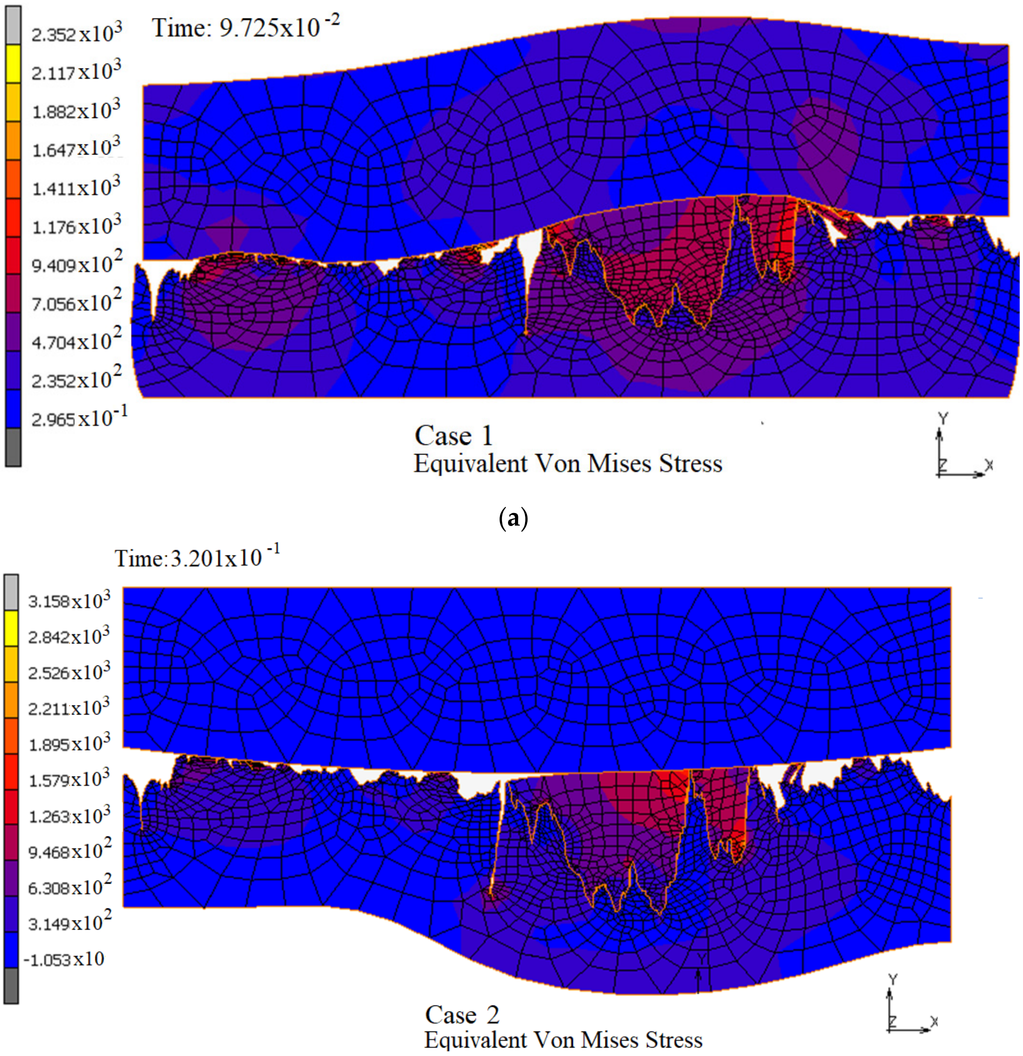

(**a**)

(**b**)

Figure 9. Distribution of reduced Huber–Mises stresses: (**a**) a curved surface (deformable) and surface after cooperation (deformable), (**b**) a curved surface (rigid) and surface after cooperation (deformable).

Table 1. 2D model: reduced Huber–Mises stresses [MPa].

Worn Surface	
Rigid/Deformable	**Deformable/Deformable**
3158	2352

In a first stage, tribological tests were performed on the samples. The specimens were then analyzed microscopically to explain the main causes of the wear mechanism. Based on the microscopic analysis, discrepancies between dry and wet contact could be examined. Figure 10 shows the illustrative surfaces after performing the tribological test. During the tests, it was observed that there are discrepancies in the wear process on the friction surface. The cracks that are found to appear in the case of wet contact cause ragged flakes protruding upwards. At dry contact, the phenomenon of wear pitting does not occur (Figure 10a,b).

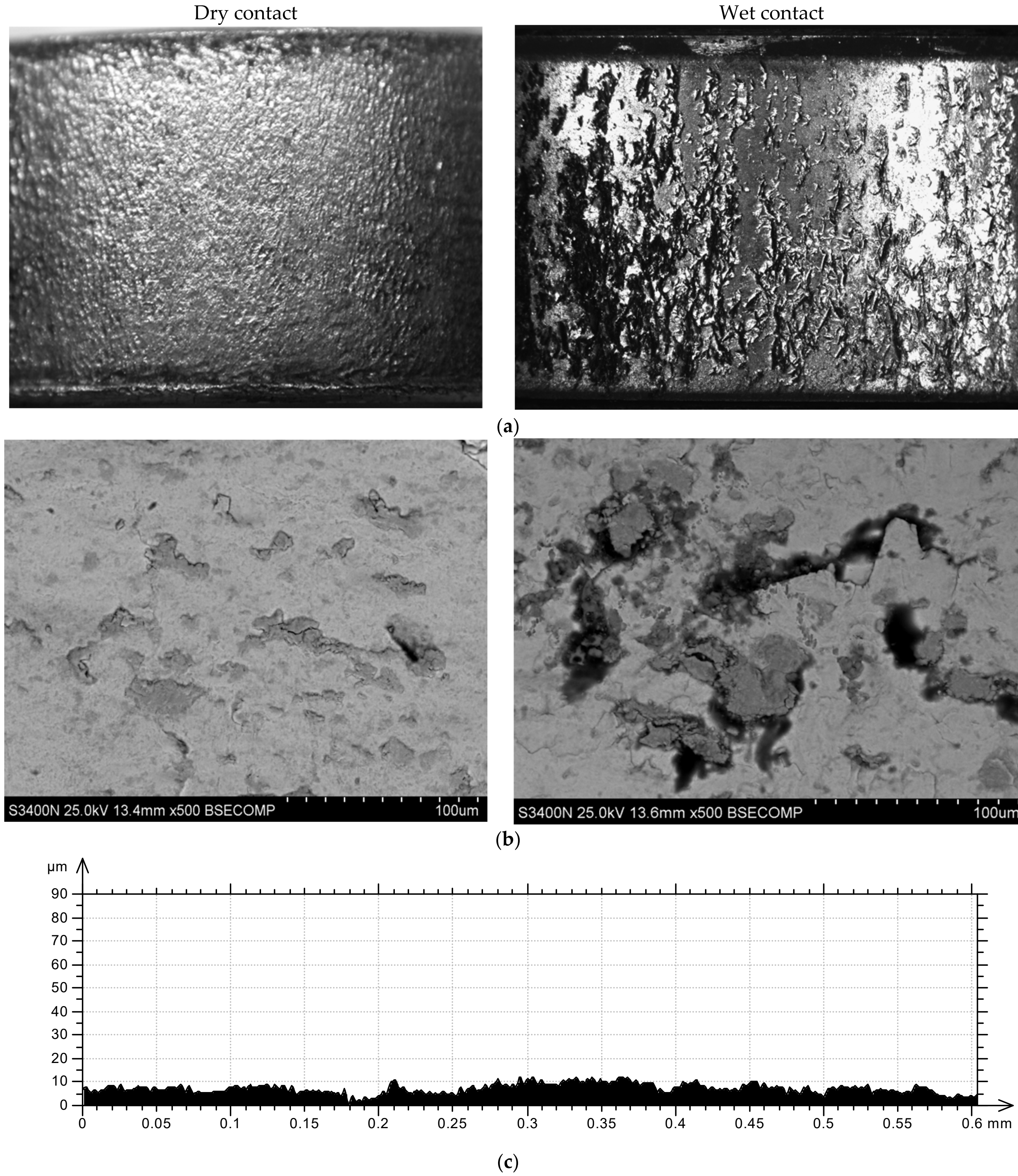

Figure 10. *Cont*.

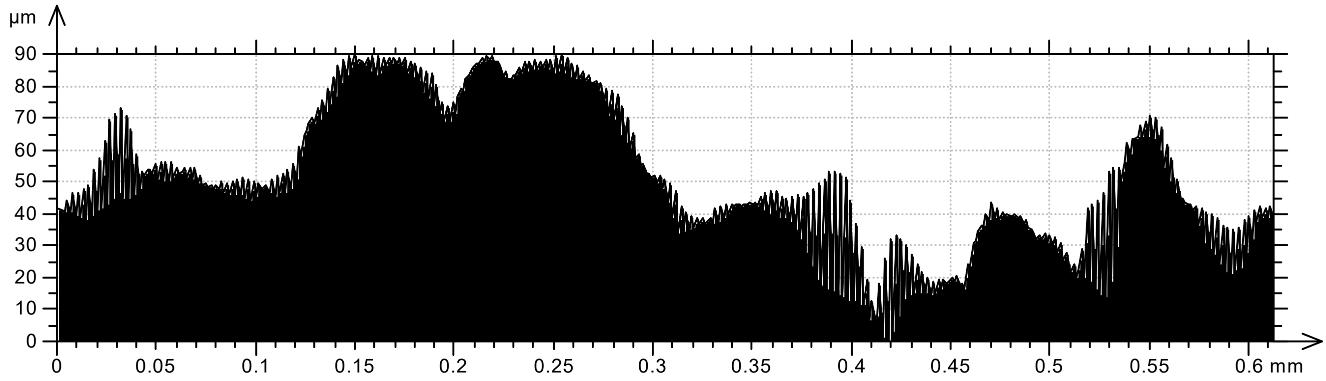

(**d**)

Figure 10. Friction surface after rubbing: (**a**) stereomicroscope, (**b**) SEM microscope, (**c**) surface topography in a dry contact, (**d**) surface topography in a wet contact.

If the friction surface in a wet contact shows roughness and cracks, it leads to further propagation of cracks. If the water pressure is high, this can lead to the development of large craters on the surface. Figure 11 shows the wear mechanism in case of rolling/sliding contact between the wheel–rail.

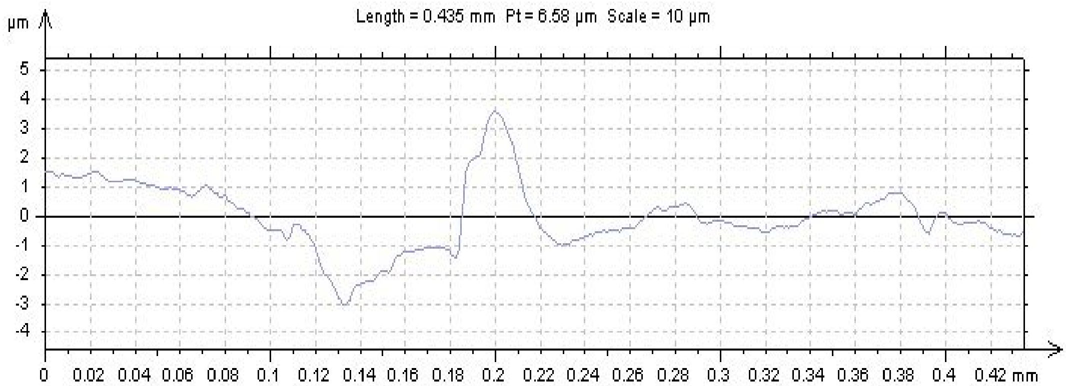

(**a**)

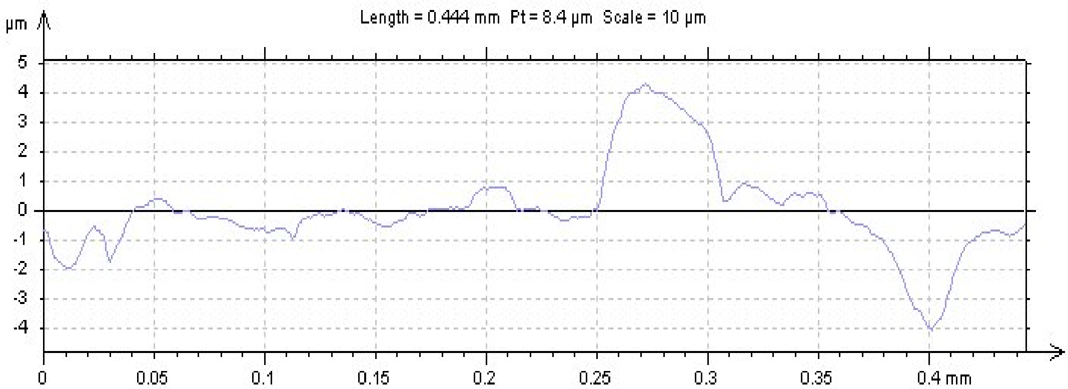

(**b**)

Figure 11. *Cont.*

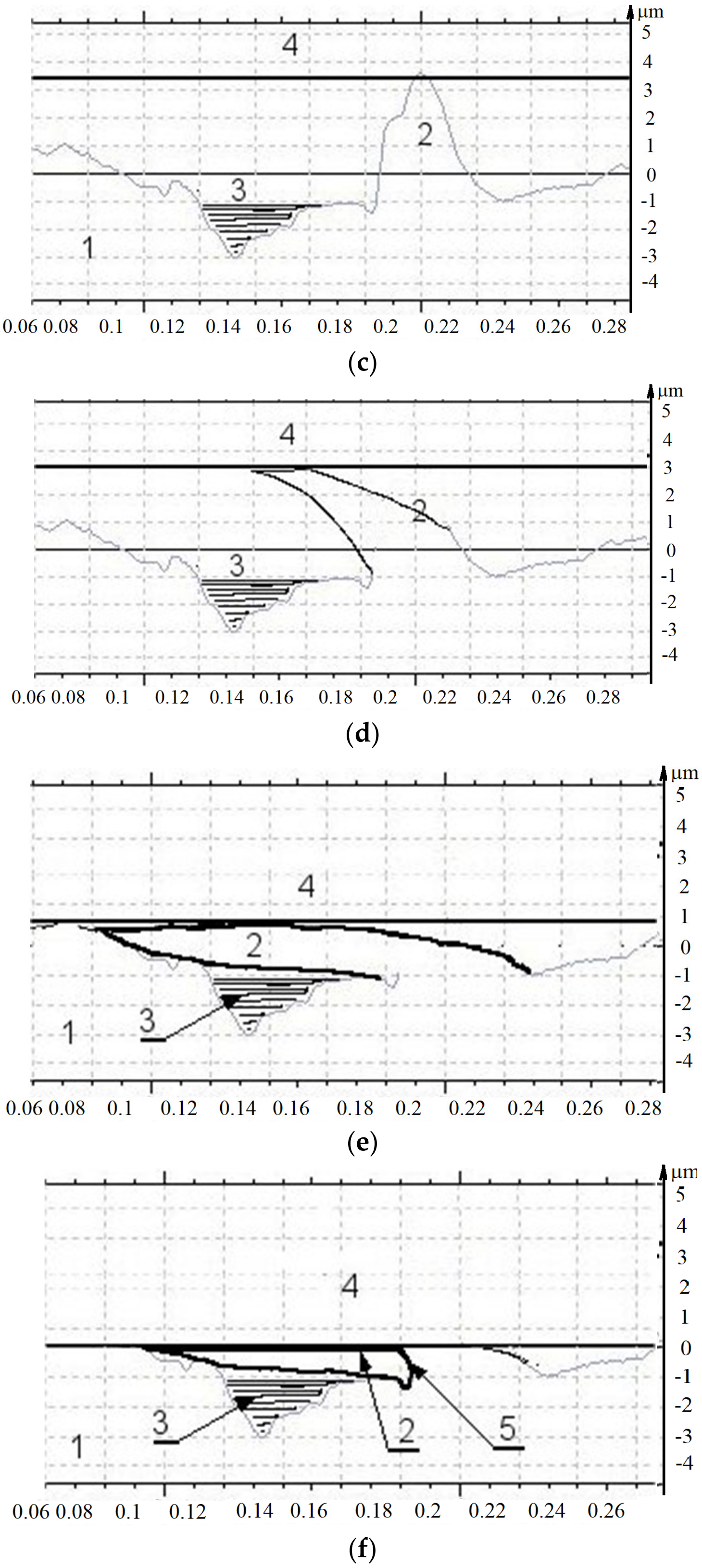

Figure 11. The wear mechanism in rolling–sliding contact: 1—railway rail, 2—roughness, 3—liquid reservoir, 4—railway wheel; (**a**,**b**) roughness profile, (**c**) filling the crater with liquid, (**d**) appearance the wear debris or roughness, (**e**) closing the fluid in the gap, (**f**) pressing the wheel against the surface.

The mechanism of wear and propagation of fatigue cracks is shown in Figure 8.

4. Discussion and Conclusions

Numerical analyses allow one to explain the mechanism of wear and determine local stress values. FEM proved to be a useful tool to identify the areas of special wear hazard. FEM can be used to explain the mechanism of wear in selected operational conditions.

In the paper, we modeled the real contact area and the relationship between the analyzed friction surface and its susceptibility to mechanical damage.

The following conclusions can be formulated:

- Destruction of the surface layer in rolling–sliding contact takes the form of the delamination wear mechanism in the form of the flake wear debris,
- Propagation of cracks is on the depth and from the surface, research has proven this,
- Numerical analysis (FEM) allows one to explain the mechanism of wear and determine the local stress values,
- The obtained results of operational investigations prove that cracks and spallings of the micro and macro scale appear in areas with maximum stress and deformation,
- FEM is the right tool used to identify the areas of special wear hazard; in addition, this method also helps to explain the wear mechanisms and determine the characterization of wear, depending on the selected operational conditions,
- The depth of residual stress can be determined and correlated with the thickness of the obtained flake wear debris appearing on the surface,
- It is advisable to monitor the execution of the state of the mobile device surface layer for the diagnostic criteria proposed in this paper.

Author Contributions: Conceptualization, A.J. and H.B.; methodology, A.J. and H.B.; software, A.J. and H.B.; validation, A.J., H.B., I.S. and S.V.; formal analysis, A.J. and H.B.; investigation, A.J. and H.B.; resources, A.J. and H.B.; data curation, A.J. and H.B.; writing—original draft preparation, A.J. and H.B.; writing—review and editing, A.J. and H.B.; visualization, A.J., H.B., I.S. and S.V.; supervision, A.J., H.B., I.S. and S.V.; project administration, A.J. and H.B.; funding acquisition, A.J., H.B., I.S. and S.V. All authors have read and agreed to the published version of the manuscript.

Funding: The APC was funded by Transilvania University of Brasov.

Institutional Review Board Statement: Not applicable.

Informed Consent Statement: Not applicable.

Data Availability Statement: Not applicable.

Conflicts of Interest: The authors declare no conflict of interest.

References

1. Gallardo-Hernandez, E.A.; Lewis, R. Twin disc assessment of wheel/rail adhesion. *Wear* **2008**, *265*, 1309–1316. [CrossRef]
2. Robles Hernándeza, F.; Demasc, N.; Gonzalesa, K.; Polycarpouc, A. Correlation between laboratory ball-on-disk and full-scale rail performance tests. *Wear* **2011**, *270*, 479–491. [CrossRef]
3. Zakharov, S.; Komarovsky, I.; Zharov, I. Wheel flange/rail head wear simulation. *Wear* **1998**, *215*, 18–24. [CrossRef]
4. Garnier, B.J. *Podstawy Klimatologii*; IMGW: Warszawa, Poland, 1996.
5. Matsudaa, H.; Satohb, Y.; Kanematsub, Y.; Iwafuchib, K. On-site investigation and analysis of flaking damage leading to rail break. *Wear* **2011**, *271*, 168–173. [CrossRef]
6. Clayton, P. Predicting the wear of rails on curves from laboratory data. *Wear* **1995**, *181–183*, 11–19. [CrossRef]
7. Jin, X.; Xiao, X.; Wen, Z.; Guo, J.; Zhu, M. An investigation into the effect of train curving on wear and contact stresses of wheel and rail. *Tribol. Int.* **2009**, *42*, 475–490. [CrossRef]
8. Stocka, R.; Pippan, R. RCF and wear in theory and practice—The influence of rail grade on wear and RCF. *Wear* **2011**, *271*, 125–133. [CrossRef]
9. Lee, M.; Polycarpou, A. Microscale experimental and modeling wear studies of rail steels. *Wear* **2011**, *271*, 1174–1180. [CrossRef]
10. Kvarda, D.; Galas, R.; Omasta, M.; Shi, L.; Ding, H.; Wang, W.; Krupka, I.; Hartl, M. Asperity-based model for prediction of traction in water-contaminated wheel-rail contact. *Tribol. Int.* **2021**, *157*, 106900. [CrossRef]
11. Fasihi, P.; Kendall, O.; Abrahams, R.; Mutton, P.; Lai, Q.; Qiu, C.; Yan, W. Effect of graphite and MoS_2 based solid lubricants for application at wheel-rail interface on the wear mechanism and surface morphology of hypereutectoid rails. *Tribol. Int.* **2021**, *157*, 106886. [CrossRef]

12. Biazon, L.; Ferrer, B.P.; Toro, A.; Cousseau, T. Correlations between rail grease formulation and friction, wear and RCF of a wheel/rail tribological pair. *Tribol. Int.* **2021**, *153*, 106566. [CrossRef]
13. Shi, L.B.; Wang, C.; Ding, H.H.; Kvarda, D.; Galas, R.; Omasta, M.; Wang, W.J.; Liu, Q.Y.; Hartl, M. Laboratory investigation on the particle-size effects in railway sanding: Comparisons between standard sand and its micro fragments. *Tribol. Int.* **2020**, *146*, 106259. [CrossRef]
14. Zhu, Y.; Olofsson, U.; Soderberg, A. Adhesion modeling in the wheel–rail contact under dry and lubricated conditions using measured 3D surfaces. *Tribol. Int.* **2013**, *61*, 1–10. [CrossRef]
15. Ma, L.; Shi, L.B.; Guo, J.; Liu, Q.Y.; Wang, W.J. On the wear and damage characteristics of rail material under low temperature environment condition. *Wear* **2018**, *394*, 149–158. [CrossRef]
16. Wu, B.; Wen, Z.; Wang, H.; Jin, X. Numerical analysis on wheel/rail adhesion under mixed contamination of oil and water with surface roughness. *Wear* **2014**, *314*, 140–147. [CrossRef]
17. Sundh, J.; Olofsson, U. Relating contact temperature and wear transitions in a wheel–rail contact. *Wear* **2011**, *271*, 78–85. [CrossRef]
18. Tomberger, C.; Dietmaier, P.; Sextroc, W.; Six, K. Friction in wheel–rail contact: A model comprising interfacial fluids, surface roughness and temperature. *Wear* **2011**, *271*, 2–12. [CrossRef]
19. Scutaru, M.L.; Vlase, S.; Marin, M.; Modrea, A. New analytical method based on dynamic response of planar mechanical elastic systems. *Bound. Value Probl.* **2020**, *2020*, 104. [CrossRef]
20. Stocka, R.; Eadie, D.T.; Elvidge, D.; Oldknow, K. Influencing rolling contact fatigue through top of rail friction modifier application—A full scale wheel–rail test rig study. *Wear* **2011**, *271*, 134–142. [CrossRef]
21. Sudaa, Y.; Kominea, H.; Matsumoto, K.; Endo, Y.; Nakai, T.; Tanimoto, M. Feedback friction control between wheel and rail by detecting yaw moment of wheelset. *Wear* **2008**, *265*, 1512–1517. [CrossRef]
22. Huang, Y.B.; Shi, L.B.; Zhao, X.J.; Cai, Z.B.; Liu, Q.Y.; Wang, W.J. On the formation and damage mechanism of rolling contact fatigue surface cracks of wheel/rail under the dry condition. *Wear* **2018**, *400*, 62–73. [CrossRef]
23. Ekberg, A.; Åkesson, B.; Kabo, E. Wheel/rail rolling contact fatigue—Probe, predict, prevent. *Wear* **2014**, *314*, 2–12. [CrossRef]
24. Rong, K.; Xiao, Y.; Shen, M.; Zhao, H.; Wang, W.-J.; Xiong, G. Influence of ambient humidity on the adhesion and damage behavior of wheel–rail interface under hot weather condition. *Wear* **2021**, *486–487*, 204091. [CrossRef]
25. Al-Maliki, H.; Meierhofer, A.; Trummer, G.; Lewis, R.; Six, K. A new approach for modelling mild and severe wear in wheel-rail contacts. *Wear* **2021**, *476*, 203761. [CrossRef]
26. Lewisa, R.; Christoforoua, P.; Wangb, W.J.; Beaglesa, A.; Burstowc, M.; Lewis, S.R. Investigation of the influence of rail hardness on the wear of rail and wheel materials under dry conditions (ICRI wear mapping project). *Wear* **2019**, *430–431*, 383–392. [CrossRef]
27. Chen, H.; Furuya, T.; Fukagai, S.; Saga, S.; Ikoma, J.; Kimura, K.; Suzumura, J. Wheel slip/Slide and low adhesion caused by fallen leaves. *Wear* **2020**, *446–447*, 203187. [CrossRef]
28. Maya-Johnson, S.; Santa, J.F.; Toro, A. Dry and lubricated wear of rail steel under rolling contact fatigue—Wear mechanisms and crack growth. *Wear* **2017**, *380–381*, 240–250. [CrossRef]
29. He, C.G.; Guo, J.; Liu, Q.Y.; Wang, W.J. Experimental investigation on the effect of operating speeds on wear and rolling contact fatigue damage of wheel materials. *Wear* **2016**, *364–365*, 257–269. [CrossRef]
30. Murakami, T.; Watanabe, S.; Hirano, F. Photoelastic Study of Rolling-Sliding Contact. *J. Jpn. Soc. Lubr. Eng.* **1975**, *20*, 176–181.
31. Ichimaru, K. Asperity Interaction in Rolling Sliding Contacts. *J. Jpn. Soc. Lubr. Eng.* **1982**, *27*, 86–92.
32. Hooke, C.J. Roughness in rolling-sliding EHL contacts. *Proc. Inst. Mech. Eng. Part J.-J. Eng. Tribol.* **2006**, *220*, 338–348. [CrossRef]
33. Beagley, T.M. Severe Wear of Rolling-Sliding Contacts. *Wear* **1976**, *36*, 317–335. [CrossRef]
34. Kannel, J.W.; Tevaarwerk, J.L. Subsurface Stress Evaluations under Rolling Sliding Contacts. *Mech. Eng.* **1983**, *105*, 93–98. [CrossRef]
35. Miyakawa, Y.; Mizuno, S. Study on Rolling-Sliding Friction and Wear Properties of Solid Lubricants. 1. Rolling-Sliding Friction Properties of Unlubricated Steels. *J. Jpn. Soc. Tribol.* **1990**, *35*, 899–906.
36. Garnham, J.E.; Brightlinge, J.R.; Beynon, J.H. Rolling Sliding Dry Wear Testing—A Vibration Analysis. *Wear* **1988**, *124*, 45–63. [CrossRef]
37. Sui, P.C.; Sadeghi, F. Thermoelastic Effects in Lubricated Rolling Sliding Line Contacts. *J. Tribol.-Trans. ASME* **1991**, *113*, 174–191. [CrossRef]
38. Akazawa, M.; Kato, K. Wear Properties of SI3N4 in Rolling-Sliding Contact. *Wear* **1988**, *124*, 123–132. [CrossRef]
39. Matsumoto, S.; Nakamura, H.; Takeda, K. Temperature and Scoring of Rolling-Sliding Contact Surface. *J. Jpn. Soc. Lubr. Eng.* **1976**, *21*, 580–588.
40. Ma, L.; He, C.G.; Zhao, X.J.; Guo, J.; Zhu, Y.; Wang, W.J.; Liu, Q.Y.; Jin, X.S. Study on wear and rolling contact fatigue behaviors of wheel/rail materials under different slip ratio conditions. *Wear* **2016**, *366–367*, 13–26. [CrossRef]
41. Chen, H.; Fukagai, S.; Sone, Y.; Ban, T.; Namura, A. Assessment of lubricant applied to wheel/rail interface in curves. *Wear* **2014**, *314*, 228–235. [CrossRef]
42. Hubbard, P.D.; Farhat, N.; Ward, C.P.; Amarantidis, G.A. Contact force estimation in the wheel/rail interface for curving scenarios through regions of reduced adhesion. *Mechatronics* **2018**, *50*, 321–327. [CrossRef]